Irfan[1], Davide Astiaso Garcia[1], Massimiliano Della Pietra[2], Stefano Frangini[2], Khurram Imran Khan[3]

Synthesis, Characterization and Electrochemical Testing of MnO_2, Fe_3O_4 and Fe_3O_4-MnO_2 Hybrid Electrocatalysts in Alkaline water for fuel Cell applications

[1]Department of Astronautical Electrical and Energy Engineering, Sapienza University of Rome
Email: irfan.chemicalengg@gmail.com, Email: davide.astiasogarcia@uniroma1.it
[2]Department of Energy Technologies and Renewable Sources, Laboratory for Hydrogen and new Energy Vectors (TERIN-DEC-H2V), ENEA Italian National Agency for Energy, New Technologies and Sustainable Economic Development, C.R. Casaccia, Rome, Italy.
Email: massimiliano.dellapietra@enea.it, Email: stefano.frangini@enea.it
[3]Faculty of Materials and Chemical Engineering, GIK Institute of Engineering Sciences and Technology, Topi, KP
Email: khurram@giki.edu.pk

Corresponding Author: **Irfan**

Abstract

Efficient oxygen reduction reaction (ORR) is of critical importance in the fields of electrochemicalenergy storage and conversion, including fuel cells and batteries. The electro catalyst plays a pivotal role in facilitating the oxygen reduction reaction (ORR) and the hydrogen oxidation reaction (HOR). Manganese dioxide (MnO_2) and its composites with iron oxide (Fe_3O_4) have garnered attention as alternative electro catalysts due to their low cost, environmental friendliness, and potential for high catalytic activity. This article explores the synthesis and characterization of MnO_2, Fe_3O_4 and Fe_3O_4 –MnO_2 electro catalysts for fuel cell reactions. Up till now, the most commonly investigated ORR catalysts have been established on noble metals such as Pt which have shown better catalytic performance, but its high cost has severely limited their widespread applications. In this research work, we synthesized low-cost Fe_3O_4 and MnO_2 nanotube structure hybrid cathodecatalysts for efficient ORR using the co-precipitation method. Characterization of the prepared catalyst was made using SEM, XRD and FTIR techniques. Cyclic Voltammetry (CV), Square wave voltammetry (SWV) and electrochemical impedance spectroscopy were used for electrochemical characterization in alkaline 0.1M KOH solution. The electrochemical characterization indicated that Fe_3O_4-MnO_2, hybrid catalyst is a more efficient cathode catalyst than the other two prepared catalysts. Hence, Fe_3O_4-MnO_2 composite can be considered a good alternative to the costly platinum catalyst, for alkaline fuel cell applications.

***Keywords**: Fuel cell, Electro catalyst, Energy storage, Clean energy technology, Electrochemistry, SEM, CV*

1. Introduction

The non-renewable energy source like fossil fuel accomplishes globally the 80% energy demand across the various sector like power generation and industrial production. For instance the US has burned $1.17*10^9$ tons for electricity with a total greenhouse gas emissions of $5.026*10^9$ Tons of CO_2 equivalent in 2018 but this creates numerous ecological issues like global warming, rising sea level, and ozone layer depletion [1-3]. These issues can be resolved by increasing the use of renewable energy sources and expanding the impact of hydrogen based technologies, such as the Fuel Cells. (F.C.) system as they offer more cleaner and and more eco-friendly solutions as compared to traditional fossil fuel engines [4].

Due to the exceptional performance and versatile nature, the Polymer Electrolyte Membrane or Proton (PEM) Fuel Cell is the effective choice for portable transport and energy storage applications and inactive usage [5, 6].

In the reaction mechanism of the PEM fuel cell the hydrogen is being oxidized at anode and gives a proton that selectively permeates through a nafion perflourinated polymeric membrane while the oxygen reduction reaction (ORR) occurs at cathode. Fig. 1 shows schematically the membrane-electrode assembly (this name is commonly used to emphasize the distinctive and closely integrated structure of electrodes with the Nafion membrane) where the PEM electrochemical reactions take place. More in detail, the anode, cathode and overall reaction in the cell are as follows [7-9].assemblies and electrochemical reactions [10].

Anode Reaction:

$$H_2 \rightarrow 2H + 2e^-$$

Cathode reaction:

$$\tfrac{1}{2} O_2 + 2e^- + 2H^+ \rightarrow H_2O$$

Overall reaction:

$$H_2 + \tfrac{1}{2} O_2 + \rightarrow H_2O$$

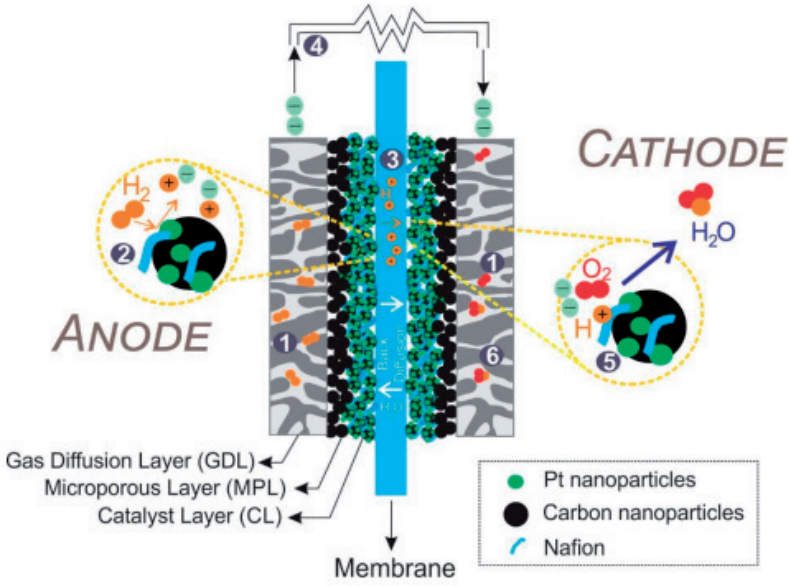

Fig.1. Schematic view of membrane electrode

To augment the ORR reaction on the cathode surface various catalysts are used like platinum (Pt) and its alloys as the Pt offers (i) high catalytic activity (ii) chemical stability (iii) high exchange current density (i_O), and (iv) optimal work function for oxidation reactions. However, the deficiency of Pt and its high cost impose efforts to reduce Pt usage to make the overall cost of PEM fuel cell more economically competitive either with combustion engines in transport or with rechargeable lithium-ion batteries in energy storage applications [8, 11].

Many researchers have investigated to develop a cost-effective catalyst like Co, Ni, Cu, Mg, Fe but the performance of these catalysts is far below the platinum performance. Most of the electrode studies focus on the ORR mechanism since the reduction of oxygen is more inactive than hydrogen oxidation, resulting typically in a 80% voltage loss on the cathode catalyst surface [12-17].

Several scientists have reported that the MnO_2 is effective and more economic cathodic electrode for ORR which could have a significant effect on the capital cost of a PEM fuel cell [18]. Similarly, the MnO_2 is used in energy applications such as primary batteries or alkaline fuel cells due to its high stability and excellent electrocatalytic properties at high pH conditions. Pt is well known to provide a high electrocatalytic activity for ORR reactions not only in acidic but also in alkaline solutions, although with some reduced efficiency. For instance, the Bacon fuel cell used in the Apollo space missions is a typical example of Pt/C catalysts used in alkaline water. Therefore, an electrochemical comparison in alkaline solutions between MnO_2 and commercial Pt/C catalysts is possible. Thus, in their studies on microbial fuel cells, Roche et al. found that power density of MnO_2 was $161*10^{-3}$ W/m^2 and comparable to a benchmark Pt/C (193 W/m^2) in neutral or moderate alkaline solution in the 7-10 PH range and at room temperature [19]. But uncertainties still remain about the effect of structure, morphology surface area and oxidation state on electrochemical activity of MnO_2 and its composites.

The others nonprecious materials like iron-based oxides (Fe_2O_3 and Fe_3O_4) are also studied as they offer an ideal option of higher efficiency, high surface area and ability on linking with Pt electro-catalysts [20, 21]. To control the demerits like un-control growth and high agglomeration, the iron-based catalysts are also unified with other transition metals like Ni, Co, Mo, and Cu to design bimetallic or composite catalysts [22].

In order to minimize the cost of PEM fuel cells and improve their durability and create a cheap and stable ORR catalyst [18]. This research focuses on alternative nonprecious catalysts based on Fe and Mn oxides. Furthermore, the ORR on the cathode is more challenging. As the Pt extensively used in the fuel cells but due to high cost and susceptibility to poisoning limit its practical application [11]. Thus, in this work wet analyzed the electrochemical behavior of three different type catalysts MnO_2, Fe_3O_4, and Fe_3O_4-MnO_2 hybrid in a dilute KOH solution. The hydrothermal technique was used for the generation of MnO_2 nanostructure, due to their economic and efficient nature. For the synthesis of Fe_3O_4 and Fe_3O_4-MnO_2 hybrid catalyst, co-precipitation was used under the inert environment. The co-precipitation process is very effective as it has high consistency, economic and offers precise particle sizes of catalysts. Consequently, these catalysts may offer the possibility of a dramatic reduction in the price of fuel cells.

2. Materials and Methods

This research employed several chemicals like $MnSO_4$. H_2O and KMnO4, $FeCl_2$, $FeSO_4$, NH_4OH, Oleic acid,

Hexanoic acid, all procured from Sigma-Aldrich Chemical Reagent Co. Ltd. These chemicals were of analytical quality and required no further purification. Distilled water was employed to prepare all solutions.

2.1. Synthesis of MnO_2 Nanostructure Catalyst

The hydrothermal method was employed for the synthesis of MnO_2. The required quantity of $MnSO_4.H_2O$ and $KMnO_4$ were dissolved in distilled water, and this solution was stirred for 2 hrs. This solution after proper mixing, heated up to 140° for 8hrs in graphite lined autoclave. To neutralize the pH, the precipitate was washed several times with distilled water. The final MnO_2 catalyst was obtained after passing through the oven at 100°C for 30 minutes.

2.2. Synthesis of Fe_3O_4 and Fe_3O_4-MnO_2 hybrid

The Fe_3O_4 was synthesized by the co-precipitation technique under the N_2 flux. In this process, $FeCl_2$ and $FeSO_4$ were mixed with a ratio of 1:3 in 100ml of distilled water in the inert environment. The NH_4OH was dropwise added to the mixture, while mixture continuously stirred at 90°C. The color of the solution was quickly changed to black. The final precipitate of Fe_3O_4 nanoparticles was washed several times with distilled water to neutralize it. The precipitate then passes through the oven at 70°C for 24hrs. A simple co-precipitation technique was employed for the hybrid catalyst (Fe_3O_4-MnO_2). After the synthesis of Fe_3O_4 by the above technique, the required quantity of MnO_2 nanoparticles and numerous coating agents were added to the mixture. The precipitate was washed several times to neutralize it and then dry at 70°C for 24hrs to get the hybrid Fe_3O_4-MnO_2 catalyst. The overall process shown in (**Fig. 2**).

The crystallite size was calculated using the Scherrer equation:

$$L = \frac{2\lambda}{\beta 2\emptyset \cos \emptyset max} \quad (1)$$

Where L is the crystal size, λ is the X-ray wavelength, $\beta_{2\theta}$ is the FWHM of the strongest peak, and θ is the Bragg angle.

This analysis confirms the successful synthesis of MnO_2, Fe_3O_4, and their hybrid with well- defined crystalline structures.

2.3. Characterization techniques

The surface morphology of prepared catalysts was studied using Field-Emission Scanning Electron Microscopy Hitachi-S-4700 (FESEM) at various magnifications from (5000-30000X) with WD 6.8mm and 100nm IQ-UNISEF. The crystallographic structure of synthesized catalysts was studied using XRD (Bruker D8 advanced diffract meter system with cu ka radiation at (1.54056Å). The functional group of prepared catalysts was studied using an FT-IR spectrometer (Thermo Nicolet, Nexus 670) with an absorption way of 32 scans and resolutions of ±4cm^{-1} with wave number from (4500-450cm^{-1}), and triglycine sulfate was used as a detector. KBr (Carlo Erba Reagent) was used as background material. The catalyst nanoparticles were mixed with KBr in the ratio of 1:20 under the pressure of 7t. Raman spectra of prepared catalysts were examined using HORIBA-LABRAM-HR Raman spectrometer with 500nm laser at room temperature.

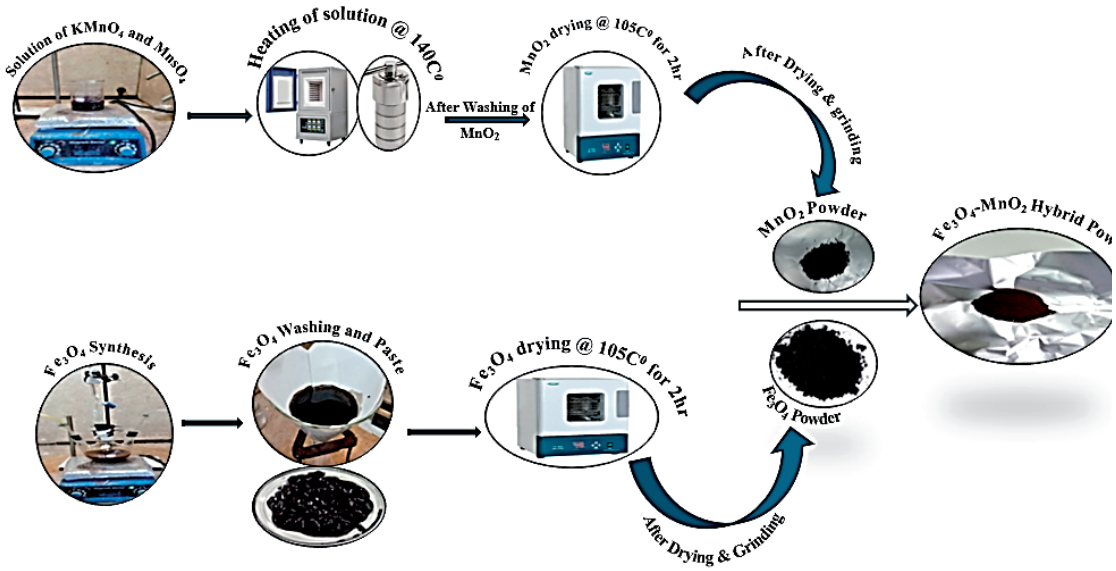

Fig. 2. Flow diagram for the synthesis of MnO_2, Fe_3O_4 and Fe_3O_4-MnO_2.

3. Results and Discussion

3.1. XRD Characterization of Catalysts

X-ray powder diffraction (XRD) was used to analyze the crystallinity and structure of the synthesized catalysts. The XRD pattern of MnO_2 (**Fig. 3a.)** confirms its pure tetragonal structure, with characteristic peaks at 2θ values of 12.3°, 28.8°, 37.6°, 41.4°, 49.8°, 56.2°, and 60.1°, corresponding to the (110), (310), (211), (301), (411), (600), and (521) planes, respectively. The average crystallite size, calculated using the Scherrer equation, was 6.93 nm. For Fe_3O_4 (**Fig. 3b.**), diffraction peaks at 2θ values of 30.2°, 35.4°, 43.45°, 53.8°, 57.3°, and 62.8° were indexed to the (220), (311), (400), (422), (511), and (440) planes, confirming a spinel cubic structure with an average crystallite size of 10.88 nm. The Fe_3O_4–MnO_2 hybrid catalyst (**Fig. 3c.)** exhibited peaks from both MnO_2 and Fe_3O_4, with a calculated crystallite size of 16.78 nm, enhancing its potential catalytic activity for oxygen reduction reactions.

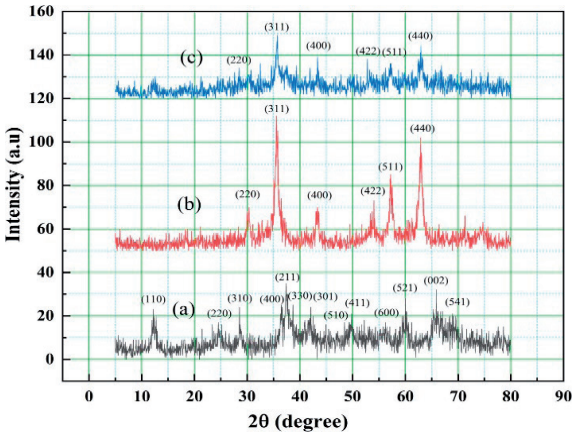

Fig. 3. X- ray diffractogram of (a) MnO_2 (b) Fe_3O_4 (c) Fe_3O_4-MnO_2

3.2. FTIR Characterization of Catalysts

Fourier Transform Infrared Spectroscopy (FTIR) was conducted to examine the functional groups in the prepared catalysts. The FTIR spectrum of MnO_2 (**Fig .4a.)** shows a broad absorption peak at 3270 cm^{-1} and a sharp peak at 1630 cm^{-1}, indicating O-H vibrational modes due to adsorbed water. In the fingerprint region, bands at 920, 725, and 505 cm^{-1} correspond to Mn-O vibrations, characteristic of MnO_2 octahedrons. The simplicity of the spectrum reflects the symmetrical structure of MnO_2. For Fe_3O_4 (**Fig .4b.**), absorption peaks at 3285 cm^{-1} and 1629 cm^{-1} are attributed to O-H vibrational modes on the surface, while the peak at 546 cm^{-1} corresponds to Fe-O bond vibrations. Peaks at 1633 cm^{-1} and 3400 cm^{-1} further confirm the presence of hydroxyl groups on the Fe_3O_4 surface.

The Fe_3O_4–MnO_2 hybrid spectrum (**Fig .4c.**) exhibits absorption bands at 3305 cm^{-1} and 1543 cm^{-1}, indicating O-H bond vibrations from both MnO_2 and Fe_3O_4. The peak at 1543 cm^{-1} also represents Mn-O and Fe-O bond vibrations, confirming the successful hybridization of the two materials.

This FTIR analysis verifies the presence of key functional groups and bonds, demonstrating the structural integrity of the synthesized catalysts.

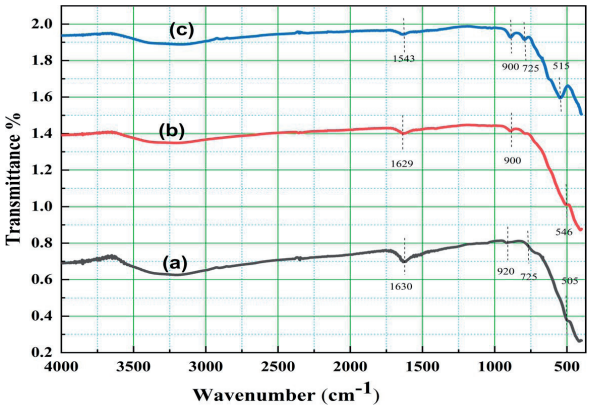

Fig. 4. FTIR spectrum of (a) MnO_2 (b) Fe_3O_4 (c) Fe_3O_4 –MnO_2

3.3. Raman Spectroscopy of Catalysts

Raman spectroscopy was employed to investigate the structural characteristics of the synthesized catalysts. The Raman spectrum of the carbon-supported MnO_2 catalyst (**Fig. 5a.**) exhibits prominent D and G bands at 1344 cm^{-1} and 3100 cm^{-1}, respectively. A broad peak at 3500 cm^{-1} also corresponds to the G band, indicating a higher MnO_2-to-carbon ratio and confirming the significant MnO_2 content on the carbon support.

For Fe_3O_4 (**Fig. 5b.**), characteristic peaks were observed at 298 cm^{-1} and 380 cm^{-1}, along with a smaller peak at 1250 cm^{-1}. These peaks suggest the valence change between trivalent and divalent iron ions, confirming the Fe_3O_4 structure. The Raman spectrum of the Fe_3O_4–MnO_2 hybrid (**Fig. 5c.**) shows peaks at 600 cm^{-1} and 3100 cm^{-1}, though with reduced intensity in the D and G bands. This indicates a decrease in the sp^2 domain and increased structural disorder, likely due to the effective embedding of Fe_3O_4 within the MnO_2 matrix. The Raman analysis highlights the structural features and interactions between the components of the synthesized catalysts.

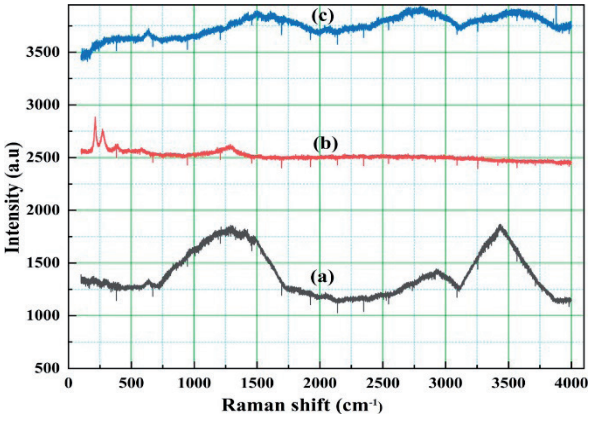

Fig. 5. Raman Spectroscopy of (a) MnO_2 (b) Fe_3O_4 (c) Fe_3O_4–MnO_2

3.4. Morphology of the catalyst (FE-SEM)

The surface morphology of the synthesized catalysts was analyzed using FE-SEM. The MnO_2 catalyst, prepared via hydrothermal treatment for 8 hours, exhibits a unique flower-like whisker structure (**Fig. 6a.**). With extended treatment, the whiskers grow larger, forming plate-like morphologies interspersed with nanorods (**Fig. 6b.**). This nanostructure significantly enhances surface area, improving electron transfer and oxygen adsorption capabilities. The FE-SEM image of Fe_3O_4 (**Fig. 6c.**) reveals spherical nanoparticles with good dispersity and an average diameter of ~15 nm. The size distribution is narrow, controlled through reaction parameters, but some agglomeration occurs due to self-assembly of nuclei. Larger particles result from temperature-induced growth and precursor ratio adjustments during co-precipitation synthesis.

The Fe_3O_4–MnO_2 hybrid morphology (**Fig. 6d.**) combines features of both MnO_2 and Fe_3O_4. The hybrid displays porous plate-like and nanorod structures of MnO_2 interspersed with spherical Fe_3O_4 particles. This structure is expected to provide a synergistic effect, leveraging the high surface area of MnO_2 and the magnetic properties of Fe_3O_4 to enhance catalytic performance.

3.5. Electrochemical Characterizations test

The faradic current efficiency and capacitive performance of the prepared catalyst were investigated through cyclic voltammetry. The experiments were carried out on Gamry reference 3000 potentiostat. Three electrode assemblies were employed with Pt wire and Ag/AgCl acting as a counter and reference electrode, respectively.

A glassy carbon electrode coated with catalyst ink formed the working electrode (electrode area 0.64cm^2). The ink was prepared by dissolving a 7.6mg catalyst in distilled water and, applied to the electrodes, dried overnight at atmospheric temperature. The electrolyte for the setup was 0.1M KOH solution. Gamry Software was used for Electrochemical Testing. Fig.7 shows the Gamry electrochemical apparatus used in this work.

3.6. Cyclic Voltammetry test

(**Fig .8.**) represents the cyclic voltammogram for MnO_2, Fe_3O_4, and Fe_3O_4 -MnO_2 observed for potential window (-0.6-0.2V) at 50 mVs^{-1} scan rate. A quasi-rectangular pattern is observed for all three catalysts indicating the excel

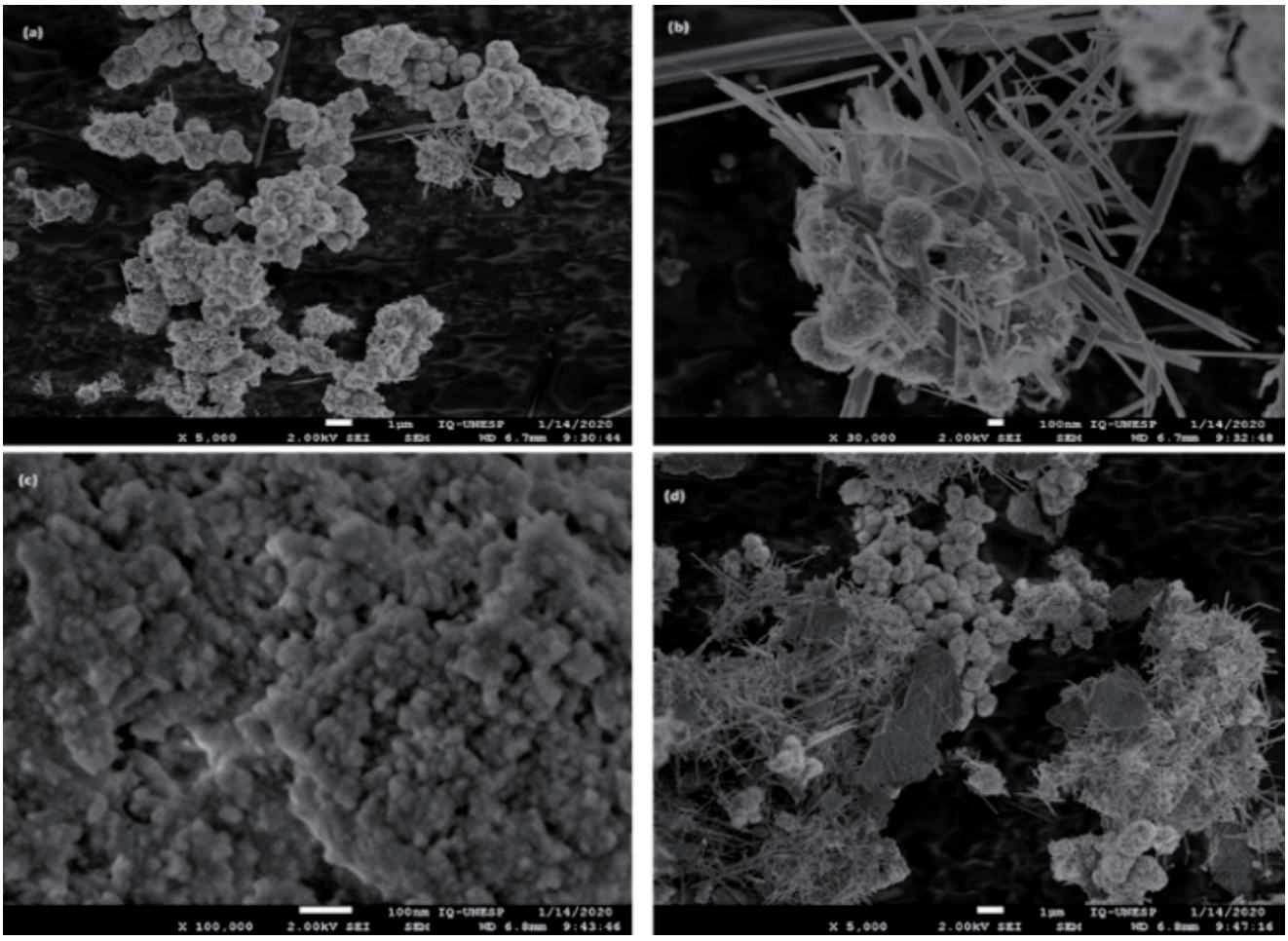

Fig. 6. FE-SEM images of (a-b) MnO_2 (c) Fe_3O_4 (d) Fe_3O_4 –MnO_2

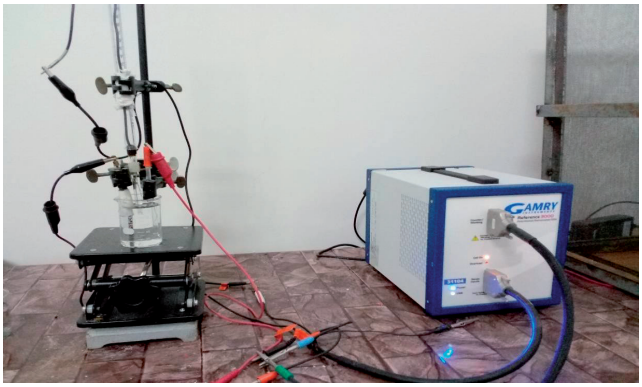

Fig. 7. Gamry Software for Electrochemical Testing.

lent capacitive nature of material. The anodic peak current values of $9.2*10^{-7}$A, $4.2*10^{-7}$A, and $5.6*10^{-7}$A at a potential of 0.2 V were observed for MnO_2, Fe_3O_4, and Fe_3O_4-MnO_2, respectively. The cathode peak current values of -2.4 $*10^{-6}$A at -0.58 V, $-9.4*10^{-7}$A at -0.59 V, and $-1.3*10^{-6}$A at –0.39 V were noted for MnO_2, Fe_3O_4, and Fe_3O_4-MnO_2, respectively.

3.7. Square wave voltammetry (SWV)

To understand the active site Fe_3O_4-MnO_2 hybrid catalysis the swv voltammetry method is used. It can avoid effect with double layer charging current overwhelms the faradic currents by SWV oxidation and reduction of species is registered as a peak or trough in the current signals at the potential at which the species begins to be oxidized or reduced. Moreover, it has excellent sensitivity and rejection of background current. In this work the net current results are presented using a cumulative voltammogram approach. Cumulative SWV is essentially an integration procedure in which each net current is the sum of all previous net currents. The resulting plot is a sigmoid curve, which replaces the conventional peak-shaped SWV curve. An advantage of cumulative SWV vs conventional SWV is that it reports the two most important voltammetric parameters (i.e. half-wave potential ($E_{1/2}$) and limiting current) with a better sensitivity. Figure 9 reports the commulative SWV curves of the MnO_2, Fe_3O_4, and Fe_3O_4-MnO_2. The curves were acquired starting from 0.25 to 1.25 Volt vs Ag/AgCl. Pulse size was 20 mV and frequency was 10 Hz, which means that duration of each pulse was 50 ms. All the three materials show an half-wave potential at about 0.82 V (vs the Ag/AgCl reference electrode), which is characteristic of the Fe^{+2}/Fe^{+3} redox couple. However the SWV result of Fe_3O_4- MnO_2 is highly different from MnO_2 and Fe_3O_4. for what is concerned the limiting current parameter. Limiting current at anodic potentials where oxidation reactions occur is higher in the case of the composite Fe_3O_4- MnO_2 as compared to the single material catalysts. Good limiting current at cathodic potential where the ORR reactions occur, is also observable, although the best result was obtained with the single Fe_3O_4 catalyst. Therefore composite Fe_3O_4-MnO_2 can be used as an efficient cathode catalyst in Alkaline fuel cells.

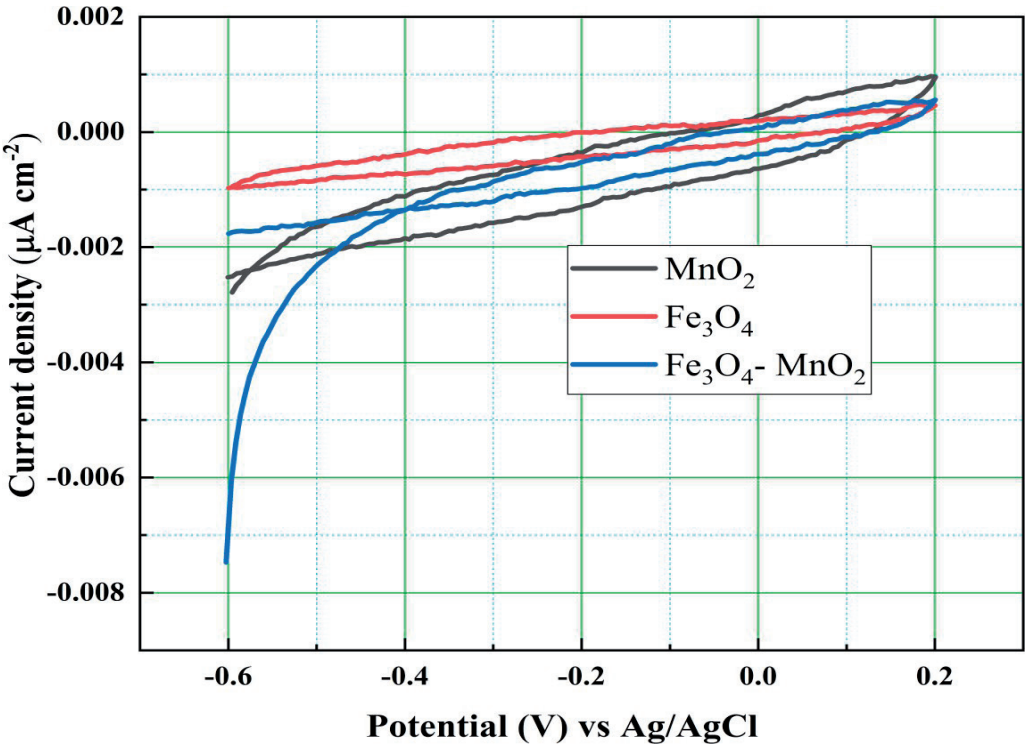

Fig. 8. Cyclic voltammetry of (a) MnO_2 (b) Fe_3O_4 (c) Fe_3O_4 –MnO_2 at 50mVs^{-1}.

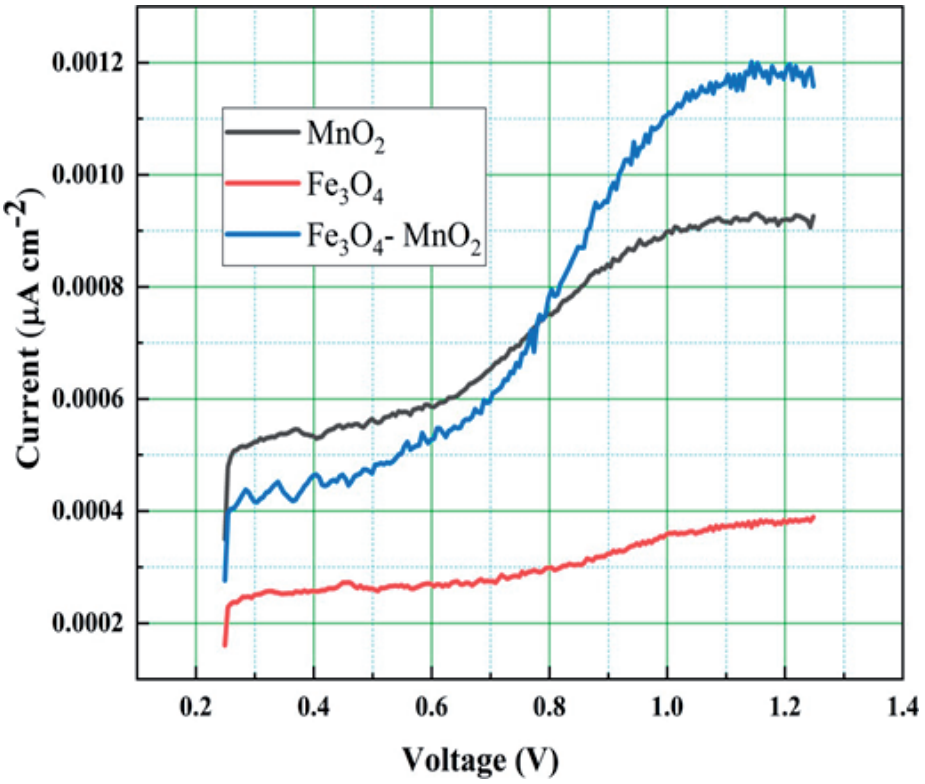

Fig. 9. Square wave voltammetry of (a) MnO_2 (b) Fe_3O_4 (c) Fe_3O_4-MnO_2

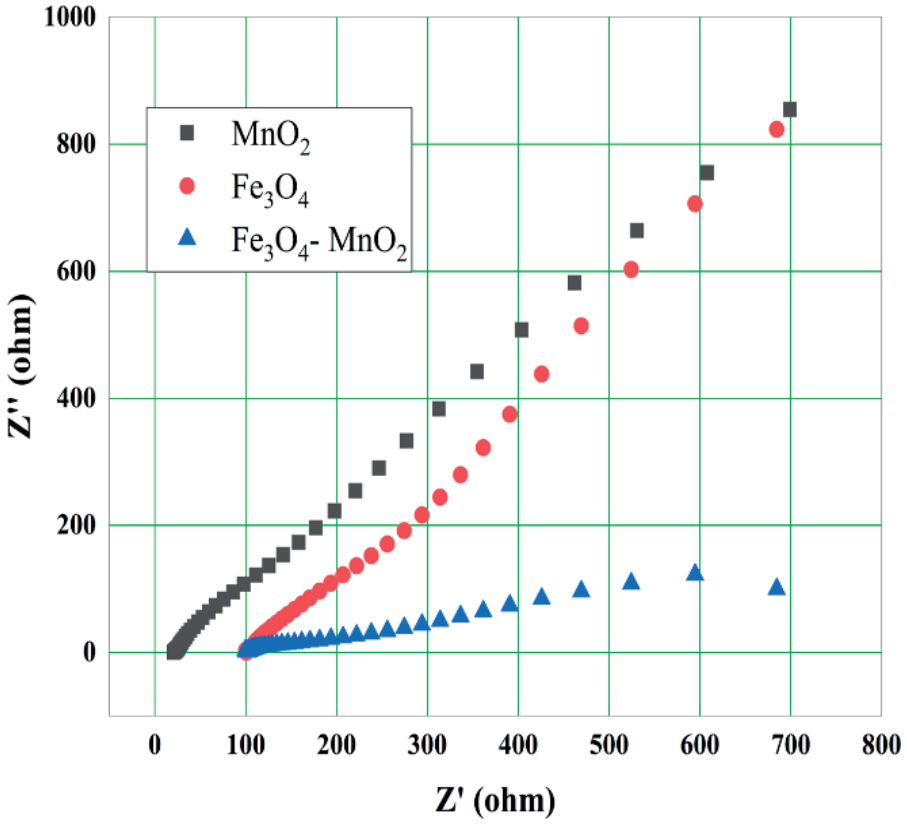

Fig. 10. Electrochemical impedance spectroscopy of (a) MnO_2 (b) Fe_3O_4 (c) Fe_3O_4- MnO_2

3.8. Electrochemical Impedance Spectroscopy (EIS)

The charge transfer resistance of the prepared catalyst was examined through electrochemical impedance spectroscopy (EIS), as shown in (**Fig. 10**). The same three-electrode system and electrolyte were used as in the CV study. The EIS was performed at an Ac voltage amplitude of 10mV in the frequency range from 105Hz to 0.1Hz. The charge transfer impedance of MnO2- Fe_3O_4 was significantly lower than the values observed for Fe_3O_4 and MnO_2. The trend indicates that the reaction of Fe_3O_4-MnO_2 was faster than MnO_2 and Fe_3O_4. Hence, the electrochemical performance of the Fe_3O_4-MnO_2 was remarkably superior to MnO_2 and Fe_3O_4. This elevates its status as the perfect candidate to replace Pt/C electrocatalysts for improving the ORR reaction in Alkaline fuel cells.

Conclusion

In this research work, we synthesized Fe_3O_4-MnO_2 hybrid electro catalyst using the co- precipitation method for cathode side reaction in Alkaline fuel cell. The hybrid catalysts have a simple preparation technique with good electrochemical activities

Electrochemical Impedance Spectroscopy (EIS) studies show that the charge transfer impedance of MnO_2-Fe_3O_4 was significantly lower than the values observed for Fe_3O_4 and MnO_2 indicating higher electrocatalytic activity. Ease of preparation, low cost of material, and its excellent electrochemical performance could make this electro catalyst a promising and stable catalyst. Therefore, it can be a better alternative to the platinum catalyst as an electrode for scaling up and commercializing for practical applications. The Fe_3O_4-MnO_2 composite exhibit remarkable high ORR activity and has a good stability. These results suggest that Fe_3O_4-MnO_2 has potential catalyst of the oxygen reduction reaction.

References

[1] Pehlivan-Davis, S., *Polymer Electrolyte Membrane (PEM) fuel cell seals durability*. 2016, Loughborough University United Kingdom.

[2] Kumar, S., *Fuzzy logic based driving pattern recognition for hybrid electric vehicle energy management*. 2015: Arizona State University.

[3] Policy, U.S.E.P.A.O.o., *Inventory of US Greenhouse Gas Emissions and Sinks: 1990-1994*. 1995: US Environmental Protection Agency.

[4] Shirsath, A.V., et al., *Electrochemical pressure impedance spectroscopy applied to polymer electrolyte membrane fuel cells for investigation of transport phenomena.* Electrochimica Acta, 2020. **363**: p. 137157.

[5] Haile, S.M., et al., *Solid acids as fuel cell electrolytes.* Nature, 2001. **410**(6831): p. 910-913.

[6] Nam, J.H., et al., *Microporous layer for water morphology control in PEMFC.* International Journal of Heat and Mass Transfer, 2009. **52**(11-12): p. 2779-2791.

[7] Kim, J., et al., *Modeling of proton exchange membrane fuel cell performance with an empirical equation.* Journal of the electrochemical society, 1995. **142**(8): p. 2670.

[8] Sharma, S. and B.G. Pollet, *Support materials for PEMFC and DMFC electrocatalysts—A review.* Journal of Power Sources, 2012. **208**: p. 96-119.

[9] Wang, C.-H., et al., *Cobalt–iron (II, III) oxide hybrid catalysis with enhanced catalytic activities for oxygen reduction in anion exchange membrane fuel cell.* Journal of Power Sources, 2015. **277**: p. 147-154.

[10] Nørskov, J.K., et al., *Origin of the overpotential for oxygen reduction at a fuel-cell cathode.* The Journal of Physical Chemistry B, 2004. **108**(46): p. 17886-17892.

[11] Cho, Y.-H., et al., *Effect of platinum amount in carbon supported platinum catalyst on performance of polymer electrolyte membrane fuel cell.* Journal of Power Sources, 2007. **172**(1): p. 89-93.

[12] Tasic, G.S., et al., *Non-noble metal catalyst for a future Pt free PEMFC.* Electrochemistry Communications, 2009. **11**(11): p. 2097-2100.

[13] Yoon, Y.-G., et al., *A multi-layer structured cathode for the PEMFC.* Journal of power sources, 2003. **118**(1-2): p. 189-192.

[14] Rao, C.V., et al., *High temperature polymer electrolyte membrane fuel cell performance of PtxCoy/C cathodes.* Journal of Power Sources, 2010. **195**(11): p. 3425-3430.

[15] Feng, X. and Y. Wang, *Multi-layer configuration for the cathode electrode of polymer electrolyte fuel cell.* Electrochimica acta, 2010. **55**(15): p. 4579-4586.

[16] Zhou, T. and H. Liu, *Effects of the electrical resistances of the GDL in a PEM fuel cell.* Journal of Power Sources, 2006. **161**(1): p. 444-453.

[17] Yu, X. and S. Ye, *Recent advances in activity and durability enhancement of Pt/C catalytic cathode in PEMFC: Part I. Physico-chemical and electronic interaction between Pt and carbon support, and activity enhancement of Pt/C catalyst.* Journal of power sources, 2007. **172**(1): p. 133-144.

[18] Larminie, J., A. Dicks, and M.S. McDonald, *Fuel cell systems explained*. Vol. 2. 2003: J. Wiley Chichester, UK.

[19] Roche, I., K. Katuri, and K. Scott, *A microbial fuel cell using manganese oxide oxygen reduction catalysts.* Journal of Applied Electrochemistry, 2010. **40**: p. 13-21.

[20] Dhali, S., et al., *Pd-Fe2O3 decorated nitrogen-doped reduced graphene oxide/CNT nanohybridas electrocatalyst for proton exchange membrane fuel cell.* Diamond and Related Materials, 2022. **126**: p. 109115.

[21] Ravichandran, S., et al., *Pt nanoparticles decorated on Fe2O3/N, P-doped mesoporous carbon for enhanced oxygen reduction activity and durability.* Journal of Electrochemical Energy Conversion and Storage, 2021. **18**(2): p. 021006.

[22] Zhang, G., et al., *Preparation of Fe3O4/rebar graphene composite via solvothermal route as binder free anode for lithium ion batteries.* Journal of Alloys and Compounds, 2016. **661**: p. 448-454.

URL:http://www.oreillynet.com/pub/a/oreilly/tim/news/2005/09/30/what-is-web-20.html?page=1 (29.2.2009.) – internet citation example

Engineering Power – *Bulletin of the Croatian Academy of Engineering* Vol. 19(4) 2024 – ISSN 1331-7210 (Print)
ISSN 2718-322X (Online)
Publisher: Croatian Academy of Engineering (HATZ), 28 Kačić Street, P.O. Box 14, HR-10000 Zagreb, Republic of Croatia
Editor-in-Chief: Prof. Vedran Mornar, Ph.D., President of the Academy
University of Zagreb, Faculty of Electrical Engineering and Computing
Editor: Prof. Bruno Zelić, Ph.D., Vice-President of the Academy
University of Zagreb, Faculty of Chemical Engineering and Technology
Guest Editor: Prof. Neven Duić, Ph.D., University of Zagreb, Faculty of Mechanical Engineering and Naval Architecture
Activities Editor: Tanja Miškić Rogić
Editorial Board: Prof. Vedran Mornar, Ph.D., Prof. Vladimir Andročec, Ph.D., Prof. Bruno Zelić, Ph.D., Assoc. Prof. Mario Bačić, Ph.D., Prof. Neven Duić, Ph.D.
Editorial Board Address: Croatian Academy of Engineering (HATZ), "Engineering Power" – Bulletin of the Croatian Academy of Engineering, Editorial Board, 28 Kačić Street, P.O. Box 14, HR-10000 Zagreb, Republic of Croatia
E-mail: hatz@hatz.hr
Graphical and Technical Editor: Tiskara Zelina, Ltd., Zelina
Press: Tiskara Zelina, Ltd., Zelina
Circulation: 200